ACS OMEGA

http://pubs.acs.org/journal/acsodf

Article

# Improvement of the Anode Properties of Lithium-Ion Batteries for $SiO_x$ with a Third Element

Tomoki Hirono, Hiroyuki Usui, Yasuhiro Domi, Wataru Irie, Toshiyuki Sawada, and Hiroki Sakaguchi*

Cite This: *ACS Omega* 2022, 7, 1223−1231

Read Online

ACCESS | Metrics & More | Article Recommendations | Supporting Information

**ABSTRACT:** Silicon oxide ($SiO_x$) has been placed into practical use as an anode active material for next-generation Li-ion batteries because it has a higher theoretical capacity than graphite anodes. However, the synthesis method is typically vapor deposition, which is expensive, and the poor electron conductivity of $SiO_x$ restricts high performance. In this study, we prepared $M/SiO_x$ active materials consisting of $SiO_x$ and a third element ($M$ = Al, B, Sn) using a low-cost mechanical milling (MM) method and investigated their electrode properties as Li-ion battery anodes. Also, the authors added a third element to improve the conductivity of the $SiO_2$ matrix. Al, B, and Sn were selected as elements that do not form a compound with Si, exist as a simple substance, and can be dispersed in $SiO_2$. As a result, we confirmed that $SiO_x$ has a nanostructure of nanocrystalline Si dispersed in an amorphous-like $SiO_2$ matrix and that the third element $M$ exists not in the nanocrystalline Si but in the $SiO_2$ matrix. The electron conductivity of $SiO_x$ was improved by the addition of B and Sn. However, it was not improved by the addition of Al. This is because $Al_2O_3$ was formed in the insulator due to the oxidization of Al. The charge−discharge cycle tests revealed that the cycle life was improved from 170 cycles to 330 or 360 cycles with the addition of B or Sn, respectively. The improvement in electron conductivity is assumed to make it possible for $SiO_2$ to react with Li ions more uniformly and form a structure that can avoid the concentration of stress due to the volume changes of Si, thereby suppressing the electrode disintegration.

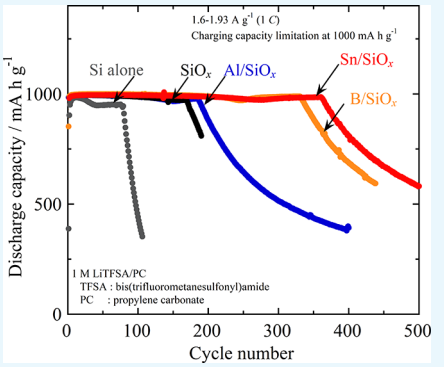


## 1. INTRODUCTION

Lithium-ion batteries have been used in many types of devices, such as power supplies for laptop computers, because they are lighter and have a higher energy density than other secondary batteries. In recent years, owing to the demands of the higher performance of portable electronic devices and the electrification of automobiles, there has been a strong demand for energy densities higher than those exhibited by conventional materials. Therefore, it is necessary to further increase the capacities of the cathode and anode materials.

Currently, graphite is used as the anode material, and its initial capacity reversibility has reached 90% or higher. In addition, it has excellent cycle properties because the volume change during charge−discharge is small. However, its theoretical capacity is only 372 mA h $g^{-1}$, and it is not expected to exceed this theoretical capacity.

Therefore, Si is an attractive active material as an anode for lithium-ion batteries because it is the same group 14 element as graphite and repeatedly alloyed and dealloyed reversibly with lithium ions. Si is an indispensable material for increasing capacity because it has a theoretical capacity (3600 mA h $g^{-1}$) that is nearly 10 times that of graphite. However, the smooth redox reaction of alloying and dealloying with lithium ions cannot be performed because the electron conductivity of Si is low, and the diffusion of lithium ions is slow. Additionally, it causes a large volumetric change of approximately 380% during lithiation and delithiation, and the stress generated at that time causes cracks in the Si particles, causing the particles to fall out of the current collector. As a result, a rapid capacity decrease occurs because the contact between the active material, surrounding Si particles, and conductive material is interrupted, the Si particles are electrically isolated, and they are not involved in the subsequent charge−discharge reaction.

To address this problem, various approaches have been carried out.[1−20] For example, it has been reported that the yield stress exceeds the stress generated during charging by setting the Si crystallite size to 10 nm or less so that the cracking of Si particles is suppressed and the cycle properties are improved. In addition, it has been reported that the cracking of Si particles can be suppressed and the cycle properties can be improved by reducing the Si particle size to 150 nm or less.[21]

As a result of such various developments, in recent years, $SiO_x$ has been installed in the anode material for Li-ion

**Received:** October 18, 2021
**Accepted:** November 30, 2021
**Published:** December 21, 2021





https://doi.org/10.1021/acsomega.1c05689
*ACS Omega* 2022, 7, 1223−1231

batteries of electric vehicles because it enables a longer driving range. $SiO_x$ has a higher capacity than the current graphite. $SiO_x$ is a mixed phase consisting of Si and $SiO_2$. Our group has previously revealed that $SiO_x$ is an amorphous material composed of a three-dimensional $SiO_4$ tetrahedral network similar to silica ($SiO_2$) glass and metallic Si clusters and that the Si clusters are finely dispersed in the $SiO_4$ matrices.[22] Therefore, the $SiO_2$ matrix is considered to exhibit better cycle properties than Si alone by relaxing the stress due to volume expansion during charge and discharge of Si.[23]

However, the capacity reduction of $SiO_x$ during the charge−discharge cycle is remarkable compared to that of graphite. It is suggested that this is because the reaction with lithium ions is localized due to the poor electron conductivity of $SiO_x$ and then the active material phase cracks, eventually leading to electrode collapse. Therefore, $SiO_x$ used in the anode material of electric vehicles is also utilized as an anode material composed of a mixture with graphite. In the future, it is expected that the mixing ratio of $SiO_x$ to graphite tends to increase because further increases in the driving range and extension of battery life are required. Therefore, it is necessary to improve the anode properties of $SiO_x$.

The main efforts to improve the anode properties of $SiO_x$ have involved improving Si particles and imparting conductivity. Meanwhile, there are no reports that focus on the improvement of the properties of a $SiO_2$ amorphous matrix with a third element. Therefore, the authors developed a new approach to improve the anode properties of $SiO_x$ by improving the poor electron conductivity of the $SiO_2$ matrix.

Figure 1 shows a schematic illustration of the $SiO_x$ structure designed by the authors in this study.[22] Conventional $SiO_x$ has

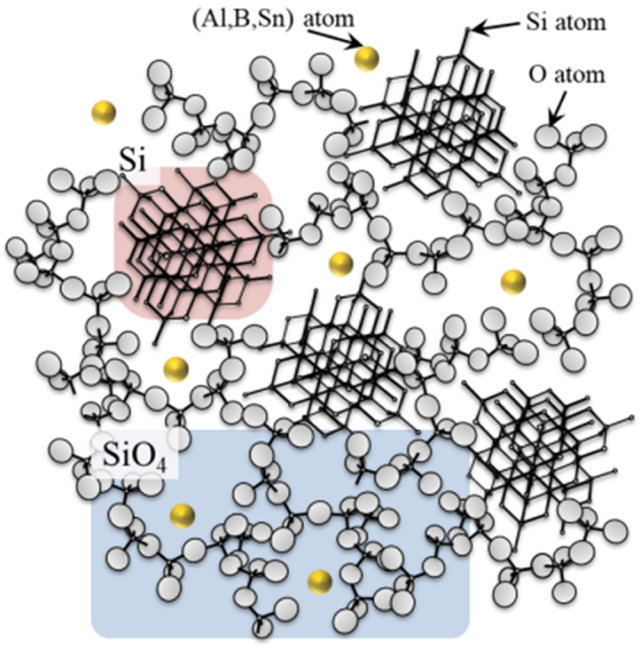


**Figure 1.** Schematic illustration of the target $SiO_x$ structure.

a structure of cluster-shaped Si dispersed in a $SiO_2$ matrix having a $SiO_4$ tetrahedral network structure. However, $SiO_2$ itself is an insulator, and its electron conductivity is quite poor at $10^{-18}$ S $cm^{-1}$. Therefore, the third element $M$ (Al, B, Sn) was added to the $SiO_4$ tetrahedral network structure. This is expected to improve the poor electron conductivity of the $SiO_2$ matrix and promote the uniform reaction of lithium ions in the $SiO_x$ electrode. Therefore, the authors thought that the damage to the electrodes was relatively small and the electrode collapse could be suppressed because the stress due to the volume expansion of Si was difficult to concentrate during charging and discharging.

Conventional $SiO_x$ is manufactured by mixing Si and $SiO_2$, heating then cooling the mixture, precipitating the generated SiO gas, and precipitating fine Si through a disproportionation reaction ($2SiO \rightarrow Si + SiO_2$).[24] However, it is extremely difficult to control the proportion of Si because the boiling point of Si (3538 K) is much higher than that of SiO (2153 K). In addition, it is difficult to precisely add other elements with different boiling points. Therefore, the authors adopted the mechanical milling method because it enables the addition of materials without going through the gas phase. In this study, we evaluated the charge−discharge properties of the anode for a lithium-ion secondary battery of an electrode made of $M/SiO_x$ prepared using the mechanical milling method and investigated the effect of the addition of the third element $M$ on the anode properties.

## 2. RESULTS AND DISCUSSION

**2.1. Observation of Powder Shape.** Figure 2 shows the scanning electron microscopy (SEM) images of $SiO_x$ and $M/SiO_x$ powders prepared using the mechanical milling method. In each case, secondary particles with a size of approximately 5 $\mu$m were observed. The secondary particles showed irregular shapes. Therefore, it can be considered that the influence of the third element on the size and shape of the secondary particles was small. Subsequently, the shapes of the primary particles could not be clearly confirmed. Therefore, the primary particles are expected to have mixed on a scale smaller than several hundred nanometers.

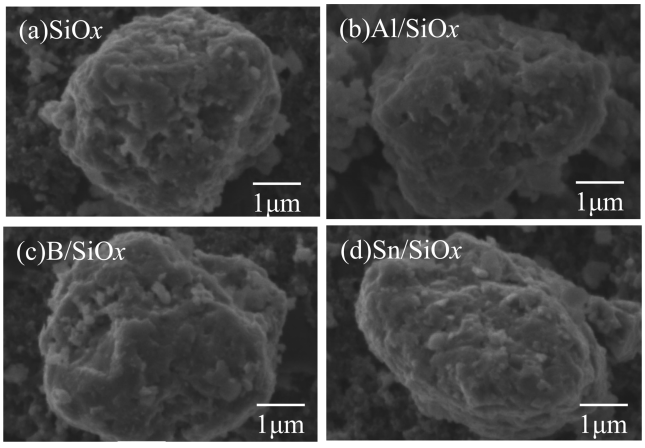


**Figure 2.** SEM images of milled $SiO_x$ and $M/SiO_x$ ($M$ = Al, B, Sn).

**2.2. Structural Analysis of Powder.** There was concern that each raw material powder would react or that the third element would dissolve in Si because of the high energy when the balls collide with each other in the powder prepared using mechanical milling. First, we checked whether the prepared material had a target structure (Figure 1). It has a structure of cluster-shaped Si dispersed in a $SiO_2$ matrix in which the third element (Al, B, Sn) is dispersed.

Figure 3a shows the X-ray diffraction (XRD) patterns of the $SiO_x$ and $M/SiO_x$ powders prepared using mechanical milling.


https://doi.org/10.1021/acsomega.1c05689
ACS Omega 2022, 7, 1223−1231

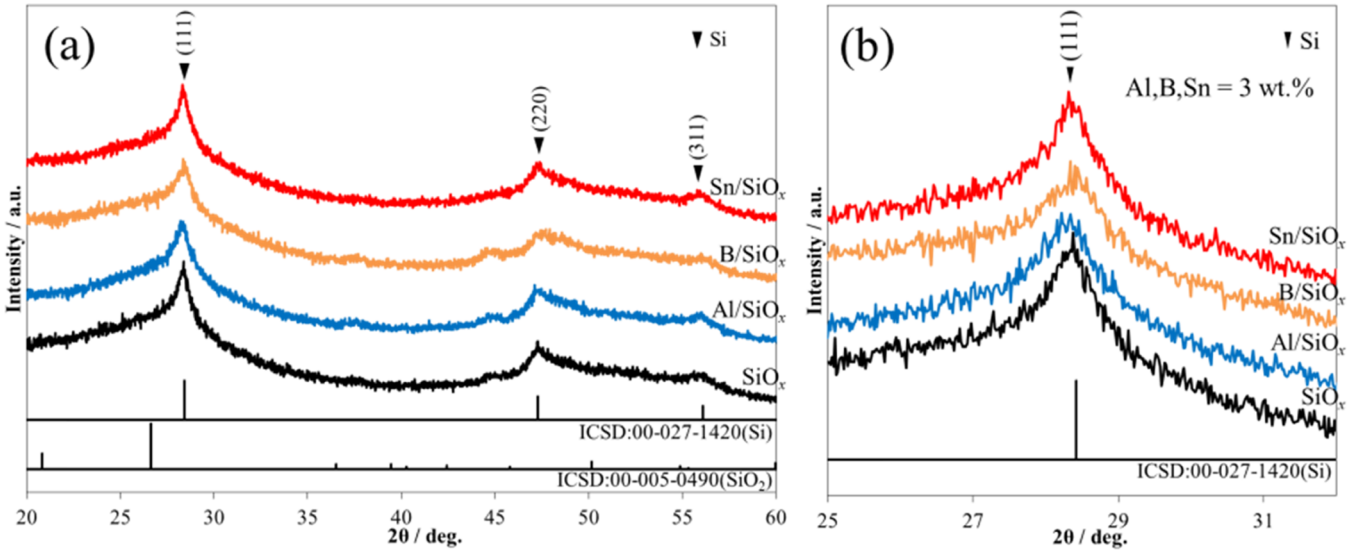


**Figure 3.** X-ray diffraction patterns of milled $SiO_x$ and $M/SiO_x$ ($M$ = Al, B, Sn) powders in the diffraction angle ranges of (a) 20−60° and (b) 25−32°.

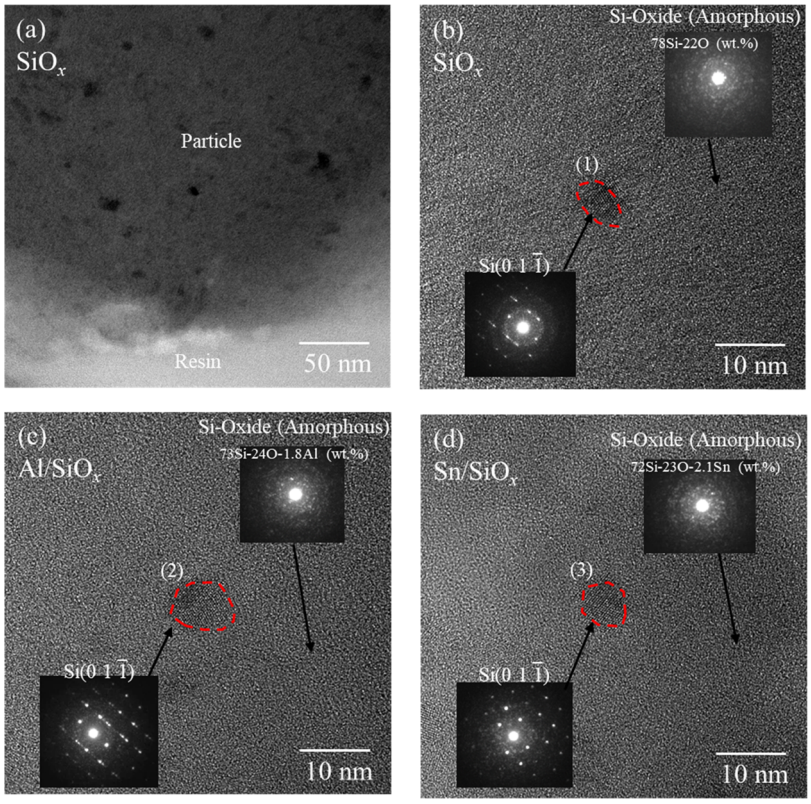


**Figure 4.** Transmission electron microscopy (TEM) images of a milled $SiO_x$ particle at (a) low magnification and (b) high magnification, and (c) $Al/SiO_x$ and (d) $Sn/SiO_x$ particles at high magnification.

The Si diffraction peaks of (111), (220), and (311) were observed for all of the powders. The crystallite size of these Si was calculated from the Scherrer equation and was found to be approximately 8−12 nm. In contrast, the diffraction peak of $SiO_2$ did not appear. This is probably because $SiO_2$ became amorphous-like owing to the high-energy milling of the mechanical milling.

Regarding the third element, the diffraction peaks of elemental substances, derivative compounds, oxides, etc. were not confirmed. First, we investigated the Si diffraction peak of (111) at approximately 28° that the third element was not dissolved in Si to disperse the third element in the $SiO_2$ matrix. Figure 3b shows the X-ray diffraction pattern in the range of 25−32° of $SiO_x$ and $M/SiO_x$ ($M$ = Al, B, Sn) powders. If the third element is dissolved in Si, the crystal lattice of Si should expand or contract and the diffraction peak should shift to the low- or high-angle side.[25] However, by comparing the powder with and without the addition of the third element, it was found that the position of the Si diffraction peak (111) at approximately 28° did not change at all. Thus, it is considered


https://doi.org/10.1021/acsomega.1c05689
ACS Omega 2022, 7, 1223−1231

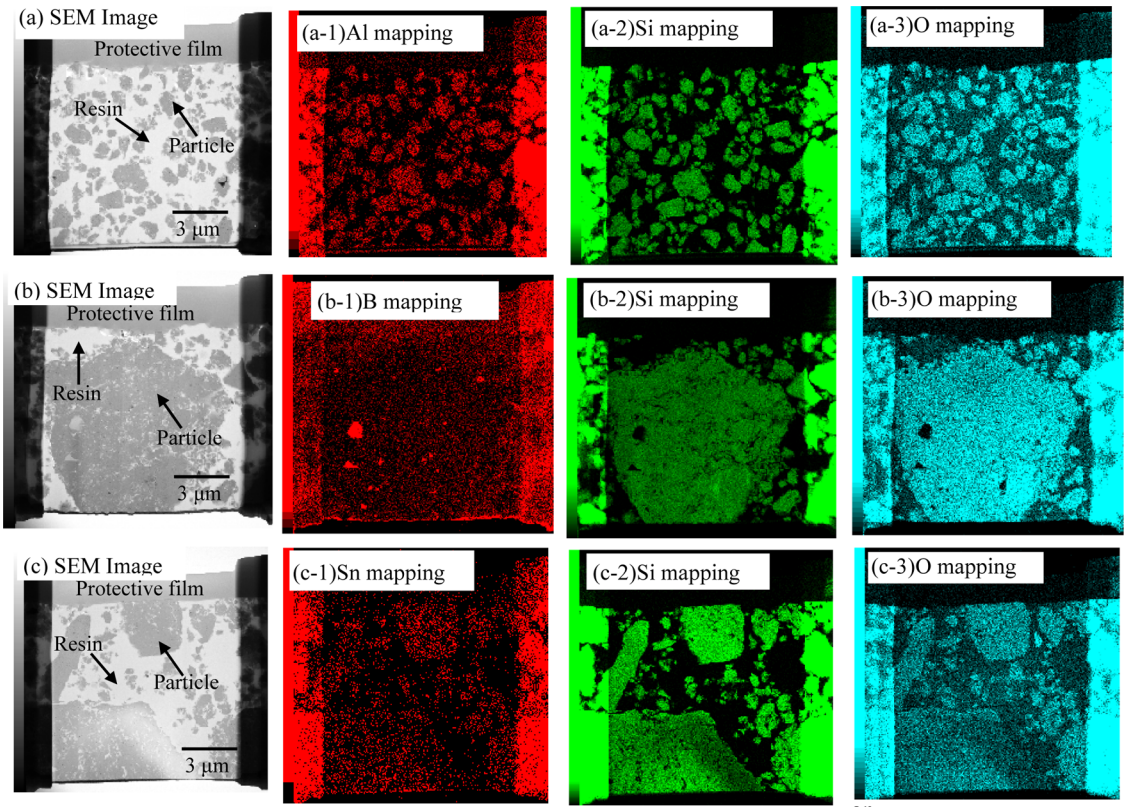


**Figure 5.** TEM images and EDS mappings of milled (a) Al/$SiO_x$, (b) B/$SiO_x$, and (c) Sn/$SiO_x$ particles.

that the third element was not dissolved in Si, but it became amorphous and existed in the $SiO_2$ matrix as intended.

From these results, it was confirmed that the powder with the third element prepared using mechanical milling was composed of amorphous-like $SiO_2$ and nanocrystalline Si, and the third element was not present in Si.

Furthermore, the structures of the prepared powders were analyzed. Figure 4a shows a low-magnification bright-field image of the edge of the $SiO_x$ particles using transmission electron microscopy. It is considered that the black spot-like part in the particle is Si and the gray area is $SiO_2$. It was found that Si and $SiO_2$ were finely pulverized after the mechanical milling treatment and Si formed a structure dispersed in the $SiO_2$ matrix. Figure 4b shows a high-magnification bright-field image and electron diffraction of a $SiO_x$ powder using transmission electron microscopy. Most of the gray areas, except the black spots, showed a halo pattern. It was considered that the areas were amorphous Si oxide because energy-dispersive X-ray spectroscopy (EDS) analysis of the part revealed that Si comprised 78 wt %, while O comprised 22 wt %. On the other hand, the black spot-like part of the red dashed line part (1) was confirmed to be elemental Si using electron diffraction. It was also found that the size of the Si microcrystals was approximately 10 nm. These results support the structure in which fine Si is dispersed in an amorphous $SiO_2$ matrix, as predicted based on XRD results.

Similarly, we found that the black spot-like part of red dashed line parts (2) and (3) of the powders with third elements Al (Figure 4c) and Sn (Figure 4d) was elemental Si using electron diffraction and had a size of approximately 10 nm. Meanwhile, there was a difference in the amorphous $SiO_2$ matrix, which was confirmed in the $SiO_x$ particles. EDS analysis of these areas revealed compositions of Si 73 wt %, O 24 wt %, and Al 1.8 wt % for the Al/$SiO_x$ powder, and Si 72 wt %, O 23 wt %, and Sn 2.1 wt % for the Sn/$SiO_x$ powder. Therefore, it is highly possible that the added third element is dispersed in the amorphous $SiO_2$ matrix.

The distribution of the third element was confirmed from the bright-field image and the EDS mapping images of Al, B, and Sn of the $M/SiO_x$ particles in Figure 5. In the case of the powder with Al or Sn, elemental Al and Sn in microcrystals, such as Si, that were confirmed in Figure 4b–d were not confirmed, and it was found that Al and Sn were uniformly dispersed throughout the powder. Meanwhile, with respect to the powder with B, B was dispersed throughout the powder, but some large particles of approximately 1 $\mu$m were confirmed. It is presumed that the mechanical milling power was insufficient under the same mechanical milling conditions because B (Mohs hardness 9.5) is harder than Al (Mohs hardness 2.9) and Sn (Mohs hardness 1.8).

Figure 6 shows the measurement results of the electrical resistivity of the pressed $M/SiO_x$ powder. It was confirmed that the addition of B or Sn improved the electron conductivity by nearly an order of magnitude compared to the powder without the addition of the third element. On the other hand, the electron conductivity of the powder with Al did not improve because the electrical resistivity was equivalent to that of $SiO_x$.

The reaction Gibbs energies ($\Delta_r G^\circ$) of $Al_2O_3$, $B_2O_3$, and $SnO_2$ are −594.61, 181.25, and 340.93 kJ $mol^{-1}$, respectively.

$$3SiO_2 + 4Al \rightarrow 3Si + 2Al_2O_3$$

$$3SiO_2 + 4B \rightarrow 3Si + 2B_2O_3$$

$$SiO_2 + Sn \rightarrow Si + SnO_2$$



https://doi.org/10.1021/acsomega.1c05689
ACS Omega 2022, 7, 1223−1231

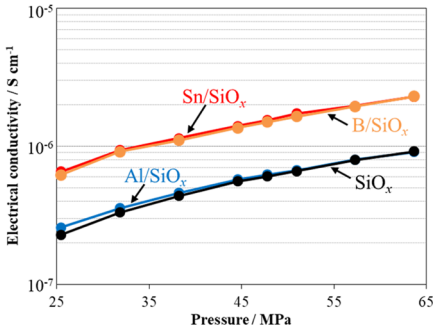


**Figure 6.** Electrical conductivity of milled $SiO_x$ and $M/SiO_x$ ($M$ = Al, B, Sn) powders under compression.

In the case of the powder with B and Sn, $\Delta_r G^\circ$ was a positive value, and it can be found that the presence of $SiO_2$ was more stable than that of $B_2O_3$ and $SnO_2$. Meanwhile, in the case of the powder with Al, $\Delta_r G^\circ$ was negative, and it can be found that the presence of $Al_2O_3$ was thermodynamically more stable than $SiO_2$. Therefore, it is presumed that $Al_2O_3$, which is an insulator, was formed because the oxidation reaction proceeded during sample preparation.

From these results, it is inferred that B and Sn[26] may have been dissolved in the $SiO_2$ matrix during the mechanical milling method.

**2.3. Charge–Discharge Properties.** Figure 7 shows the dependence of the discharge capacity of $M/SiO_x$ ($M$ = Al, B, Sn) electrodes on the cycle number in 1 M lithium bis(trifluoromethanesulfonyl)amide (LiTFSA)/propylene carbonate (PC) solution with a charge capacity limit of 1000 mA h g$(Si)^{-1}$. For comparison, the $SiO_x$ and Si electrodes were also evaluated. The Si alone electrode caused a rapid capacity decay after 100 cycles. Meanwhile, for the $SiO_x$ electrode, the capacity decay was suppressed until 170 cycles. Subsequently, in the case of the $Al/SiO_x$ electrode, the cycle properties were equivalent to those of the $SiO_x$ electrode, and the electrode performance did not improve. However, it was found that electrodes with B and Sn can achieve a longer cycle life of 150 cycles or more. It is presumed that the addition of B and Sn improved the current-collecting property of the electrodes because it improved the electron conductivity of $SiO_x$ by approximately 1 order of magnitude.

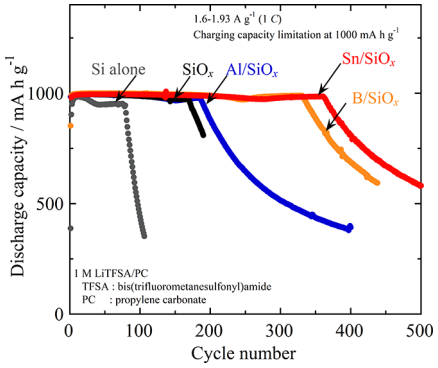


**Figure 7.** Dependence of the discharge capacity of $M/SiO_x$ ($M$ = Al, B, Sn) electrodes on cycle number in 1 M LiTFSA/PC solution with a charge capacity limit of 1000 mA h g$(Si)^{-1}$ (the result of Si alone electrode is also shown).

To determine the reason for the improvement of the electrode properties as described above, an active material consisting only of a matrix was prepared and the electrode reaction was investigated. In addition, in the $M/SiO_2$ samples, the reactivity with lithium ions due to the addition of the third element was investigated. In other words, to investigate how much lithium ions are occluded, we decided to conduct a test to examine the amount of lithium ions reacted without capacity regulation. Figure 8a shows the dependence of the discharge capacity of $SiO_2$ and $M/SiO_2$ ($M$ = Al, B, Sn) electrodes on cycle number in 1 M LiTFSA/PC at 0.38 A g$^{-1}$. The temperature and potential range for testing were set to 303 K and 0.005–2.000 V vs $Li^+/Li$, respectively. It was found that the electrodes with B and Sn showed higher capacities than those of $SiO_2$ without the addition of the third element. Originally, $SiO_2$ hardly reacted with Li ions and did not exhibit Li storage properties. However, it has recently been reported that, when $SiO_2$ becomes amorphous, the reaction

$$5SiO_2 + 4Li^+ + 4e^- \rightarrow 2Li_2Si_2O_5 + Si \quad (1)$$

proceeds, and it is possible to form silicon and lithium silicate ($Li_2Si_2O_5$), due to lithium-ion activity.[27] The authors confirmed from Figures 3 and 4 that $SiO_2$ is amorphous. In addition, the charge–discharge curves and $dQ/dV$ curves after 10 cycles were newly investigated for $SiO_2$ and $M/SiO_2$ ($M$ = Al, B, Sn) electrodes. As a result, it was found that the Si single-phase peak was observed even though these were matrix-only electrodes. In particular, it appears clearly near 0.5 V on the discharge side. This also suggests that reaction 1 is progressing. Therefore, in this study, it is considered that $SiO_2$, which became amorphous after mechanical milling, showed charge–discharge capacity. Furthermore, it is considered that the electrode with B and Sn showed higher capacity than the $SiO_2$ electrode because the reactivity with the lithium ions in the matrix was improved by the solid dissolution of B and Sn in the $SiO_2$ matrix and the uniform dispersion of B and Sn (Figure 8b). Meanwhile, it is considered that Al was oxidized and formed amorphous $Al_2O_3$, and it is dispersed in $SiO_2$ because the electron conductivity of $Al/SiO_x$ is equivalent to that of $SiO_x$. Therefore, it is presumed that the capacity of the $Al/SiO_2$ electrode did not increase because the reactivity with lithium ions could not be improved and reaction 1 was not promoted.

From these results, we consider the mechanism of extending the life of the cycle properties by adding B and Sn to $SiO_x$. Figure 9 shows a schematic illustration of the $M/SiO_x$ ($M$ = B, Sn) performance improvement mechanism. Si exhibits the following two-step lithium alloying reaction during charging.[28−31] If reaction 3 progresses, the electrode will collapse because the volume change (380%) due to the formation of $Li_{3.75}Si$ in reaction 3 is larger than the volume change (240%) due to the formation of $Li_{2.00}Si$ in reaction 2 ("$a$" in $a$-Si and $a$-$Li_{2.00}Si$ means amorphous, and "$c$" in $c$-$Li_{3.75}Si$ means crystalline).

$$a\text{-Si} + 2Li^+ + 2e^- \rightarrow a\text{-}Li_{2.00}Si \quad (2)$$

$$a\text{-}Li_{2.00}Si + 1.75Li^+ + 1.75e^- \rightarrow c\text{-}Li_{3.75}Si \quad (3)$$

In the case of a charge capacity limit of 1000 mA h g$^{-1}$, it is considered that lithium alloying of Si occurs locally because the electrodes without the addition of the third element or with the addition of Al have low reactivity with lithium ions in the $SiO_2$ matrix. As a result, $Li_{3.75}Si$, which has a large volume


https://doi.org/10.1021/acsomega.1c05689
ACS Omega 2022, 7, 1223−1231

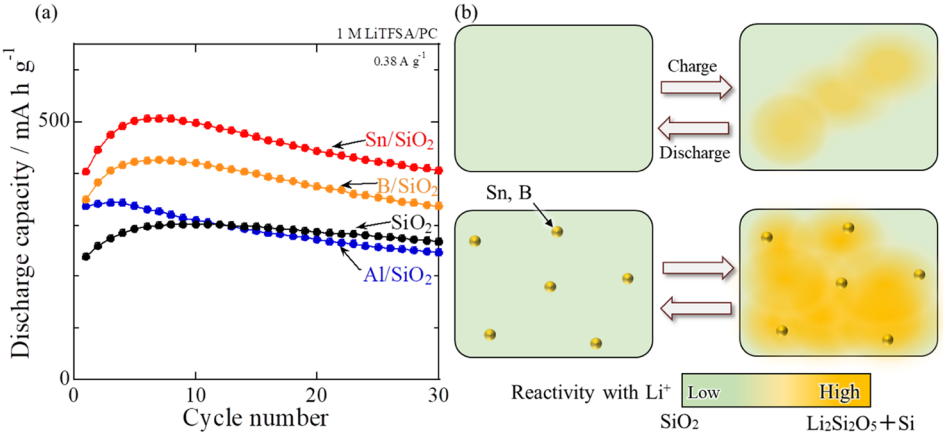


**Figure 8.** Dependence of the (a) discharge capacity of $SiO_2$ and $M/SiO_2$ ($M$ = Al, B, Sn) electrodes on cycle number in 1 M LiTFSA/PC at 0.38 A $g^{-1}$. The temperature and potential range for the testing were set to 303 K and 0.005−2.000 V vs $Li^+/Li$, respectively. (b) Schematic illustration of $SiO_2$ and $M/SiO_2$ ($M$ = B, Sn) reaction with Li ions.

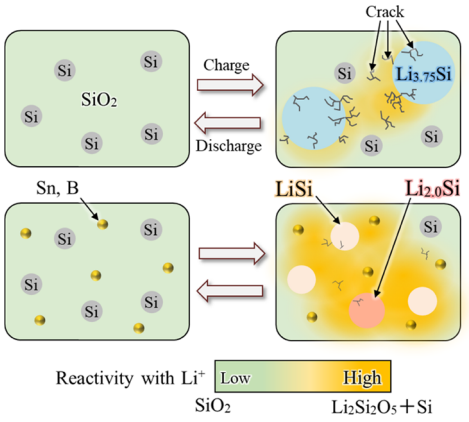


**Figure 9.** Schematic illustration of the $M/SiO_x$ ($M$ = B, Sn) performance improvement mechanism.

change, was formed, which is thought to have caused electrode collapse and capacitance decline. Meanwhile, in the case of the electrode with B or Sn, the electron conductivity was improved, and the lithium-ion reactivity of the $SiO_2$ matrix was increased. Thus, Si in the entire active material phase can easily react with lithium ions more uniformly. Therefore, it was possible to suppress the formation of $Li_{2.00}Si$, which has a small volume change. Therefore, it is considered that the electrode with B or Sn improved the cycle properties because the stress due to the volume expansion of Si was difficult to concentrate during charging, and the damage to the electrodes was relatively small and the electrode collapse could be suppressed.

## 3. CONCLUSIONS

In this study, we prepared an active material ($M/SiO_x$) with a third element ($M$ = Al, B, Sn) in $SiO_x$ using a mechanical milling method and investigated the anode properties of Li-ion batteries. We confirmed that the structure of $SiO_x$ consists of nanocrystalline Si dispersed in an amorphous-like $SiO_2$ matrix, and a third element is present in the $SiO_2$ matrix but not in the nanocrystalline Si. The electron conductivities of $B/SiO_x$ and $Sn/SiO_x$ were higher than that of $SiO_x$. Meanwhile, the electron conductivity of $Al/SiO_x$ was not higher than that of $SiO_x$. This is because $Al_2O_3$ was formed in the insulator due to the oxidization of Al. In the cycle properties test conducted with a charge (Li storage) capacity limit of 1000 mA h $g^{-1}$, it was found that the cycle life was improved from 170 cycles to 330 or 360 cycles in the powder with B or Sn, respectively. When $SiO_2$ becomes amorphous, the reaction $5SiO_2 + 4Li^+ + 4e^- \rightarrow 2Li_2Si_2O_5 + Si$ (1) proceeds, and it is possible to form silicon and lithium silicate ($Li_2Si_2O_5$), due to lithium-ion activity. The electron conductivity was improved because they were present in the matrix and B or Sn was dispersed in the $SiO_2$ matrix. Therefore, it is considered that this is because $SiO_2$ reacts uniformly with lithium ions due to the improvement of electron conductivity so that the stress due to the volume change of Si is difficult to concentrate and the destruction of the electrode is reduced.

## 4. EXPERIMENTAL SECTION

**4.1. Sample Preparation.** *4.1.1. Preparation of $SiO_x$ and $M/SiO_x$ ($M$ = Al, B, Sn) Powder.* Normal Si powder was prepared using a mass-produced gas-atomizing device. A flake-shaped Si raw material (purity 98.7%) of approximately 10−20 mm was placed in a crucible with pores of $\varphi$2.5 mm at the bottom of the crucible and heated and melted in a dry argon gas atmosphere using a high-frequency induction melting furnace. The molten metal was then discharged at 1823 K. $N_2$ gas was sprayed on the molten metal at the part directly below the pores, and it was solidified at a cooling rate of approximately $10^{0-2}$ K $s^{-1}$. As a result, a gas-atomized Si powder was obtained. This powder was classified using a sieve with an opening of 300 $\mu$m.

To prepare the $SiO_x$ powder, a mixture of the above-mentioned gas-atomized Si powder and commercially available $SiO_2$ powder (Kojundo Chemical Lab. Co. Ltd., purity 99.9%) was placed in an austenite-based stainless steel vessel together with high-carbon chromium-bearing steel (C 1%, Cr 1%) balls ($\varphi$19 mm) with a $Si:SiO_2$ weight ratio of 54:46. The amount of each powder was 32.4 g for the Si powder and 27.6 g for the $SiO_2$ powder. The weight of each ball was 12 kg. The weight ratio of the active material to the balls was 1:200.

To prepare the $M/SiO_x$ powder, a mixture of gas-atomized Si powder and commercially available $SiO_2$ powder and the third element $M$ (Al: purity 99.9%, Kojundo Chemical Lab. Co. Ltd., B: purity 99.9%, Kojundo Chemical Lab. Co. Ltd., Sn: purity 99.0%, Kojundo Chemical Lab. Co. Ltd.) was placed in an austenite-based stainless steel vessel together with high-carbon chromium-bearing steel balls with a $Si:SiO_2:M$ weight


https://doi.org/10.1021/acsomega.1c05689
ACS Omega 2022, 7, 1223−1231

ratio of 52:45:3. The amount of each powder was 31.4 g for Si powder and 26.8 g for $SiO_2$ powder and 1.8 g for *M* (Al, B, Sn) powder. The weight of each ball was 12 kg.

These vessels were sealed, the interior was evacuated to a pressure of 0.1 MPa, and dry argon gas was sealed through gas replacement. The vessel was set in a vibrating ball mill device (MB-1 type manufactured by Chuo Kakohki Co. Ltd.). After 50.4 ks of mechanical milling treatment under the specified conditions (amplitude: ± 4 mm, frequency: 1200 rpm), the number of balls was increased, the weight ratio of the active materials to the balls was 1:300, and the mechanical milling was repeated for 50.4 ks.

The obtained mechanical milling powder was adjusted to a particle size of 10 $\mu$m or less due to collisions between powders in a 0.7 MPa $N_2$ gas stream using a jet mill device (Co-Jet manufactured by SEISHIN ENTERPRISE Co. Ltd.) to crush the agglomerated powder. The target powder was obtained using this process.

*4.1.2. Preparation of M/SiO$_2$ and SiO$_2$ Powder.* For comparison, the same powder preparation was performed by adding only $SiO_2$ and the third element *M*, without adding the gas-atomized Si powder. Consequently, the change in the properties (reactivity with lithium ions) of the $SiO_2$ matrix due to the presence of the third element *M* was investigated.

Commercially available $SiO_2$ powder was weighed and placed in a zirconia vessel filled with $\varphi$5 mm zirconia balls. Additionally, $SiO_2$ powder and the third element powder (Al powder: purity 99.9% FUJIFILM Wako Pure Chemical Corporation, B powder: purity 99.0% FUJIFILM Wako Pure Chemical Corporation, Sn powder: purity 99.9%, 325 mesh RARE METALLIC Co., Ltd.) were placed in a zirconia vessel together with $\varphi$5 mm zirconia balls with a $SiO_2$:*M* weight ratio of 94:6 (powder: 1.5 g, ball: 100 g).

The vessel was then sealed and set in the Premium Line planetary ball mill device (PL-7 type). Each powder was subjected to a mechanical milling treatment ($SiO_2$: 7.2 ks, Al/$SiO_2$: 14.4 ks, B/$SiO_2$: 7.2 ks, Sn/$SiO_2$: 7.2 ks) at 380 rpm to obtain the target powder.

**4.2. Analysis of the Obtained Sample.** The Si crystallite sizes of the prepared $SiO_x$ and $M/SiO_x$ powders were measured using X-ray diffraction (XRD, RINT-2500, Rigaku Corporation, Cu K$\alpha$, 50 kV, 200 mA, 4° min$^{-1}$, 20−60°).

The morphologies of the powders were observed using a scanning electron microscope (JSM-6490LV, 5 kV, JEOL Ltd.). In addition, the prepared powders were attached to conductive tape for observation.

The size and dispersibility of nanocrystalline Si and the third elements were observed using a transmission electron microscope (JEM-F200, 200 kV, JEOL Ltd.). The preparation of the observation samples is described below. First, the prepared powder was embedded in a conductive thermosetting resin. Subsequently, a carbon-protective film was deposited on the sample surface. Finally, these samples were cut to a size of approximately 10 $\mu$m × 10 $\mu$m × thickness 100 nm using a high-performance focused ion beam device (MI4050, Mo mesh; Hitachi High-Tech Corporation) and used as an observation sample.

The electron conductivity of the obtained powder was evaluated using a powder resistivity measuring unit (MCP-PD51, Nittoseiko Analytech Co. Ltd., four-probe device). Approximately 3 g of the prepared powder was placed in a sample holder of $\varphi$10 mm and compressed to a maximum of 64 MPa to measure the volumetric electron conductivity.

**4.3. Electrode Fabrication.** $SiO_x$, $M/SiO_x$ powder, $SiO_2$, and $M/SiO_2$ powder were each mixed with acetylene black, carboxymethyl cellulose, and styrene-butadiene rubber at a weight ratio of 70:15:10:5 using a kneading machine. These were then applied on a Cu foil with a coating amount of approximately 1.0 mg cm$^{-2}$ to obtain a mixture electrode.

**4.4. Cell Assembly and Charge−Discharge Tests.** For the charge−discharge test, a 2032-type coin was constructed, composed of the above electrode as the working electrode, a Li metal sheet as the counter electrode, and a glass fiber filter as the separator. Lithium bis(trifluoromethanesulfonyl)amide (LiTFSA) dissolved in propylene carbonate (PC) was used at the concentration of 1 M. Cell assembly and electrolyte preparation were conducted in an Ar-filled glovebox (Miwa MFG, DBO-2.5LNKP-TS) with an oxygen content less than 1 ppm and dew point below 173 K. Also, the authors want to show that this material can be used in cold climates. Therefore, it is evaluated on a PC (MP 223 K), which has a lower melting point than EC (MP 311 K) and is hard to freeze.

Regarding the $SiO_x$ and $M/SiO_x$ electrodes, galvanostatic charge−discharge cycling tests were performed using an electrochemical measurement system in the potential range of 0.005−2.000 V vs $Li^+$/Li. In addition, the current density and measurement temperature were set to 1.60−1.93 A g$^{-1}$ (1C) and 303 K, respectively. Electrochemical measurements were performed with a charge limit of 1000 mA h g$^{-1}$. In this study, we considered it to be a mixture of Si and $SiO_2$ and treated $SiO_2$ as being inactive with lithium ions. The theoretical capacitance was calculated assuming that only Si reacted with lithium ions. The maximum alloying composition in this case was calculated to be $Li_{15}Si_4$. In this case, the theoretical capacity of each powder was calculated to be 1931 mA h g$^{-1}$ for $SiO_x$, 1890 mA h g$^{-1}$ for Al/$SiO_x$, 1860 mA h g$^{-1}$ for B/$SiO_x$, and 1890 mA h g$^{-1}$ for Sn/$SiO_x$. Regarding $SiO_2$ and $M/SiO_2$ electrodes, galvanostatic charge−discharge tests were performed with a potential range of 0.005−2.000 V vs $Li^+$/Li, a current density of 0.38 A g$^{-1}$, and a measurement temperature of 303 K.

## ■ ASSOCIATED CONTENT

### Supporting Information

The Supporting Information is available free of charge at https://pubs.acs.org/doi/10.1021/acsomega.1c05689.

Charge−discharge curves and d*Q*/d*V* plots (PDF)

## ■ AUTHOR INFORMATION


### Corresponding Author

**Hiroki Sakaguchi** − *Department of Chemistry and Biotechnology, Graduate School of Engineering and Center for Research on Green Sustainable Chemistry, Tottori University, Tottori 680-8552, Japan;* orcid.org/0000-0002-4125-7182; Email: sakaguch@tottori-u.ac.jp; Fax: +81-857-31-5265

### Authors

**Tomoki Hirono** − *Department of Chemistry and Biotechnology, Graduate School of Engineering and Center for Research on Green Sustainable Chemistry, Tottori University, Tottori 680-8552, Japan; Sanyo Special Steel Co., Ltd., Himeji, Hyogo 672-8677, Japan*

**Hiroyuki Usui** − *Department of Chemistry and Biotechnology, Graduate School of Engineering and Center for Research on*




https://doi.org/10.1021/acsomega.1c05689
ACS Omega 2022, 7, 1223−1231

*Green Sustainable Chemistry, Tottori University, Tottori 680-8552, Japan;* orcid.org/0000-0002-1156-0340

**Yasuhiro Domi** − *Department of Chemistry and Biotechnology, Graduate School of Engineering and Center for Research on Green Sustainable Chemistry, Tottori University, Tottori 680-8552, Japan;* orcid.org/0000-0003-3983-2202

**Wataru Irie** − *Course of Chemistry and Biotechnology, Department of Engineering, Graduate School of Sustainability Science and Center for Research on Green Sustainable Chemistry, Tottori University, Tottori 680-8552, Japan*

**Toshiyuki Sawada** − *Sanyo Special Steel Co., Ltd., Himeji, Hyogo 672-8677, Japan*

Complete contact information is available at: https://pubs.acs.org/10.1021/acsomega.1c05689

### Author Contributions

The manuscript was written through contributions of all authors.

### Notes

The authors declare no competing financial interest.

## ■ ACKNOWLEDGMENTS

This work was partially supported by the Japan Society for the Promotion of Science (JSPS) KAKENHI (grant nos. 19H02817, 19K05649, and 20H00399).

## ■ REFERENCES

(1) Domi, Y.; Usui, H.; Takemoto, Y.; Yamaguchi, K.; Sakaguchi, H. Improved Electrochemical Performance of Lanthanum Silicide/Silicon Composite Electrode with Nickel Substitution for Lithium-Ion Batteries. *J. Phys. Chem. C* **2016**, *120*, 16333−16339.

(2) Iida, T.; Hirono, T.; Shibamura, N.; Sakaguchi, H. $Mg_2Ge$/Si Composite Electrodes Prepared by Gas-Deposition as Anodes for Lithium Rechargeable Battery. *Electrochemistry* **2008**, *76*, 644−648.

(3) Sakaguchi, H.; Iida, T.; Itoh, M.; Shibamura, N.; Hirono, T. Anode Properties of $LaSi_2$/Si Composite Thick-Film Electrodes for Lithium Secondary Batteries. *IOP Conf. Ser.: Mater. Sci. Eng.* **2009**, *1*, No. 012030.

(4) Usui, H.; Nishinami, H.; Iida, T.; Sakaguchi, H. Anode Properties of Cu-Coated Si Thick Film Electrodes Prepared by Electroless Deposition and Gas-Deposition. *Electrochemistry* **2010**, *78*, 329−331.

(5) Usui, H.; Nouno, K.; Takemoto, Y.; Nakada, K.; Ishii, A.; Sakaguchi, H. Influence of Mechanical Grinding on Lithium Insertion and Extraction Properties of Iron Silicide/Silicon Composites. *J. Power Sources* **2014**, *268*, 848−852.

(6) Domi, Y.; Usui, H.; Itoh, H.; Sakaguchi, H. Electrochemical Lithiation and Delithiation Properties of Ceria-Coated Silicon Electrodes. *J. Alloys Compd.* **2017**, *695*, 2035−2039.

(7) Usui, H.; Shimizu, M.; Sakaguchi, H. Applicability of Ionic Liquid Electrolytes to $LaSi_2$/Si Composite Thick-Film Anodes in Li-Ion Battery. *J. Power Sources* **2013**, *235*, 29−35.

(8) Hou, S. C.; Su, Y. F.; Chang, C. C.; Hu, C. W.; Chen, T. Y.; Yang, S. M.; Huang, J. L. The Synergistic Effects of Combining the High Energy Mechanical Milling and Wet Milling on Si Negative Electrode Materials for Lithium Ion Battery. *J. Power Sources* **2017**, *349*, 111−120.

(9) Usui, H.; Nomura, M.; Nishino, H.; Kusatsu, M.; Murota, T.; Sakaguchi, H. Gadolinium Silicide/Silicon Composite with Excellent High-Rate Performance as Lithium-Ion Battery Anode. *Mater. Lett.* **2014**, *130*, 61−64.

(10) Usui, H.; Wasada, K.; Shimizu, M.; Sakaguchi, H. $TiO_2$/Si Composites Synthesized by Sol-Gel Method and Their Improved Electrode Performance as Li-Ion Battery Anodes. *Electrochim. Acta* **2013**, *111*, 575−580.

(11) Usui, H.; Uchida, N.; Sakaguchi, H. Improved Anode Performance of Ni-P-Coated Si Thick-Film Electrodes for Li-Ion Battery. *Electrochemistry* **2012**, *80*, 737−739.

(12) Usui, H.; Uchida, N.; Sakaguchi, H. Influence of Order in Stepwise Electroless Deposition on Anode Properties of Thick-Film Electrodes Consisting of Si Particles Coated with Ni and Cu. *J. Power Sources* **2011**, *196*, 10244−10248.

(13) Usui, H.; Shibata, M.; Nakai, K.; Sakaguchi, H. Anode Properties of Thick-Film Electrodes Prepared by Gas Deposition of Ni-Coated Si Particles. *J. Power Sources* **2011**, *196*, 2143−2148.

(14) Usui, H.; Kashiwa, Y.; Iida, T.; Sakaguchi, H. Anode Properties of Ru-Coated Si Thick Film Electrodes Prepared by Gas-Deposition. *J. Power Sources* **2010**, *195*, 3649−3654.

(15) Domi, Y.; Usui, H.; Shindo, Y.; Ando, A.; Sakaguchi, H. Lithiation and Delithiation Properties of Si-Based Electrodes Pre-Coated with a Surface Film Derived from an Ionic-Liquid Electrolyte. *Chem. Lett.* **2021**, *50*, 1041−1044.

(16) Duan, J.; Tang, X.; Dai, H.; Yang, Y.; Wu, W.; Wei, X.; Huang, Y. Building Safe Lithium-Ion Batteries for Electric Vehicles: A Review. *Electrochem. Energy Rev.* **2020**, *3*, 1−42.

(17) Xin, F.; Stanley, M. Challenges and Development of Tin-Based Anode with High Volumetric Capacity for Li-Ion. *Electrochem. Energy Rev.* **2020**, *3*, 643−655.

(18) Xia, H.; Tang, S.; Lu, L. Properties of amorphous Si thin film anodes prepared by pulsed laser deposition. *Mater. Res. Bull.* **2007**, *42*, 1301−1309.

(19) Yao, J.; Ji-Li, Y.; Qiubo, G.; Qiuying, X.; Chong, Z.; Tao, F.; Jing, X.; Hui, X. Highly Porous Mn3O4 Micro/Nanocuboids with In Situ Coated Carbon as Advanced Anode Material for Lithium-Ion Batteries. *Small* **2018**, *14*, No. 1704296.

(20) Jia, R.; Jili, Y.; Qiuying, X.; Jing, X.; Xiaohui, Z.; Shuo, S.; Teng, Z.; Hui, X. Carbon shelled porous $SnO_{2-\delta}$ nanosheet arrays as advanced anodes for lithium-ion batteries. *Energy Storage Mater.* **2018**, *13*, 303−311.

(21) Liu, X. H.; Zhong, L.; Huang, S.; Mao, S. X.; Zhu, T.; Huang, J. Y. Size-Dependent Fracture of Silicon Nanoparticles During Lithiation. *ACS Nano* **2012**, *6*, 1522−1531.

(22) Nagao, Y.; Sakaguchi, H.; Honda, H.; Fukunaga, T.; Esaka, T. Structural Analysis of Pure and Electrochemically Lithiated SiO Using Neutron Elastic Scattering. *J. Electrochem. Soc.* **2004**, *151*, A1572−A1575.

(23) Shimizu, M.; Usui, H.; Fujiwara, K.; Yamane, K.; Sakaguchi, H. Electrochemical Behavior of SiO as an Anode Material for Na-Ion Battery. *J. Alloys Compd.* **2015**, *640*, 440−443.

(24) Yasuda, K.; Kashitani, Y.; Kizaki, S.; Takeshita, K.; Fujita, T.; Shimosaki, S. Thermodynamic Analysis and Effect of Crystallinity for Silicon Monoxide Negative Electrode for Lithium Ion Batteries. *J. Power Sources* **2016**, *329*, 462−472.

(25) Domi, Y.; Usui, H.; Shimizu, M.; Kakimoto, Y.; Sakaguchi, H. Effect of Phosphorous-Doping on Electrochemical Performance of Silicon Negative Electrodes in Lithium-Ion Batteries. *ACS Appl. Mater. Interfaces* **2016**, *8*, 7125−7132.

(26) Chiodini, N.; Meinardi, F.; Morazzoni, F.; Paleari, A.; Scotti, R.; Martino, D. D. Photoluminescence of Sn-Doped $SiO_2$ Excited by Synchrotron Radiation. *J. Non-Cryst. Solids* **2000**, *261*, 1−8.

(27) Chang, W.; Park, C.; Kim, J.; Kim, Y.; Jeong, G.; Sohn, H. Quartz ($SiO_2$): a New Energy Storage Anode Material for Li-Ion Batteries. *Energy Environ. Sci.* **2012**, *5*, 6895−6899.

(28) Rohrer, J.; Albe, K. Insights into Degradation of Si Anodes from First-Principle Calculations. *J. Phys. Chem. C* **2013**, *117*, 18796−18803.

(29) Domi, Y.; Usui, H.; Ando, A.; Nishikawa, K.; Sakaguchi, H. Analysis of the Li Distribution in Si-Based Negative Electrodes for Lithium-Ion Batteries by Soft X-Ray Emission Spectroscopy. *ACS Appl. Energy Mater.* **2020**, *3*, 8619−8626.

(30) Ogata, K.; Jeon, S.; Ko, D. S.; Jung, I. S.; Kim, J. H.; Ito, K.; Kubo, Y.; Takei, K.; Saito, S.; Cho, Y. H.; Park, H.; Jang, J.; Kim, H.

G.; Kim, J. H.; Kim, Y. S.; Choi, W.; Koh, M.; Uosaki, K.; Doo, S. G.; Hwang, Y.; Han, S. Evolving Affinity Between Coulombic Reversibility and Hysteretic Phase Transformations in Nanostructured Silicon-Based Lithium-Ion Batteries. *Nat. Commun.* **2018**, *9*, No. 479.

(31) Ogata, K.; Salager, E.; Kerr, C. J.; Fraser, A. E.; Ducati, C.; Morris, A. J.; Hofmann, S.; Grey, C. P. Revealing Lithium-Silicide Phase Transformations in Nano-Structured Silicon-Based Lithium Ion Batteries via *In Situ* NMR Spectroscopy. *Nat. Commun.* **2014**, *5*, No. 3217.



https://doi.org/10.1021/acsomega.1c05689
*ACS Omega* 2022, 7, 1223−1231